RESEARCH PAPER

Combined measurement of concentration distribution and velocity field of two components in a micromixing process

Mike Wellhausen · Günter Rinke · Hainer Wackerbarth

Abstract A lot of production processes involve mixing steps. The understanding of fluid flows in mixing processes of liquid components is needed in order to develop appropriate mixers for the chemical and pharmaceutical industry. Especially mixing in microfluidic systems is a challenge due to the diffusion-based processes. A multi-lamination micromixer with chessboard outlet geometry is used to induce the mixing process. To get comprehensive information about the mixing process, the velocity profile of the fluid flow and the species concentration distribution during the mixing process should be measured. Thus, we have combined particle image velocimetry (PIV) and Raman scattering. To enable rapid detection, the Raman imaging mode is used to visualise the concentration distribution. By this setup light sheets along and orthogonal to the outlet of the micromixer are recorded and synchronized with PIV measurement. As a model system we have used water and ethanol/methanol, enabling a selective monitoring of the substances by choosing appropriate spectral areas. The PIV is recorded based on Mie scattering and fluorescence using microsphere tracers. In this study, we present a setup for determination of the velocity profile field and the spatial concentration distribution of water and ethanol/methanol in a micromixer.

M. Wellhausen (✉) · H. Wackerbarth
Laser-Laboratorium Göttingen e.V., Photonic Sensor Technology,
Hans-Adolf-Krebs-Weg 1, 37077 Göttingen, Germany
e-mail: hainer.wackerbarth@llg-ev.de

G. Rinke
Karlsruhe Institute of Technology (KIT),
Institute for Micro Process Engineering,
Hermann-von-Helmholtz-Platz 1,
76344 Eggenstein-Leopoldshafen, Germany

1 Introduction

Production processes, as well as a lot of other detection methods, require complete mixing of the reagents. The objective of mixing is to obtain a homogenous blend of two solutions in as little time as possible. This can be achieved efficiently using micromixers. At small scales mixing prevalently depends on diffusion as transport mechanism, making conventional mixing methods such as turbulence generation almost impossible. However, effective mixing is still required for a lot of microfluidic devices, with applications ranging from drug dilution to reagent introduction for chemical analysis. Effective mixing concerns the quality of a mixing process. This can be measured, e. g. with two competing chemical reactions and using UV spectroscopy (Kölbl et al. 2008).

Miniaturization of existing applications for chemical and biological processes has become very attractive over the past few years (Hunt and Wilkinson 2008). Small devices—reactors, heat exchangers, static mixers and concepts like lab-on-a-chip (Fair 2007; Hunt and Wilkinson 2008; Hüttner et al. 2011, Walowski et al. 2011)—can be fabricated in configurations scaled in millimetres and embedded with micrometer-sized channels (Hoffmann et al. 2006; Rinke et al. 2011a, b). The miniaturization of reaction systems offers a lot of advantages over conventional bench top systems such as small samples and reduced waste volumes, automated sample preparations and reduced reaction time (Janasek et al. 2006). Due to the miniaturization, the detection volume in microchannels is small. Furthermore, in industry, the efficient mass and heat

transfer of micro heat exchangers are important and often a greater selectivity and higher yield for chemical reactions can be reached.

In this study, an industry-oriented multi-lamination micromixer is employed. Other research groups often work with T-shaped micromixers (Hoffmann et al. 2006; Bothe et al. 2006; Lindken et al. 2006; Mouheb et al. 2011) or cross-channel geometry (Devasenathipathy et al. 2003; Mouheb et al. 2011).

In order to obtain a better understanding of the physical and chemical processes within such components and to optimise these devices, it is necessary to monitor the concentrations within the microchannels during the mixing process. For such a purpose, optical methods are suitable. Due to the strongly increasing interest in microfluidic devices, there is a growing demand for new diagnostic tools for the analysis of flow structures, mixture formation and reaction behaviour. In particular, non-intrusive measurement techniques which do not influence the flow and reaction processes in the channels are badly needed. Several reviews are concerned with miscellaneous detection techniques (Mogensen et al. 2004; Sinton 2004; Viskari and Landers 2006).

In former reports, examples have been given for the investigation of microchannels by means of spectroscopic Raman methods. Raman scattering provides specific spectral and quantitative information about molecules (Sauter 1996). The Raman spectra are fingerprints of the molecules and their intensity is proportional to the concentration of the species. A Raman microscope is used to observe the mixing processes of chloroform and methylene chloride within a commercially available micro device (Salmon et al. 2005). Another research group applied both confocal fluorescence spectroscopy and Raman spectroscopy to monitor the mixing processes of ethanol and iso-propanol in a micromixer (Park et al. 2004). A commercial Raman microscope was used to monitor the concentration profiles during the synthesis of ethyl acetate within a micromixer, which consists of silicon and Pyrex (Fletcher et al. 2003). Some more applications emerge in the literature dealing with this issue (Lee et al. 2003; Leung et al. 2005; Ewinger et al. 2008). However, in these approaches only the spectral information or their temporal evolutions have been used.

Recording a Raman spectrum is time-consuming. An option is the Raman imaging mode, where a selective spectral area representing vibrational modes of one species is chosen to monitor its concentration locally instead of recording the whole spectrum. Characteristic spectral areas are chosen by spectral filters to enable a rapid detection in the imaging mode. This approach was carried out to characterise fuel sprays (Bazile and Stepowski 1994; Malarski et al. 2006). Raman-based determination of concentration gradients of mixing solvents is of fundamental importance in the field of fuel cell research, especially in the case of methanol and water (Deabate et al. 2008). One of the first investigations using the Raman imaging mode applied to a model of a multi-lamination mixer was pursued in our group by Beushausen et al. (2009).

In addition to the concentration and the mixing ratio, respectively, the local flow velocity and direction are of interest in the analysis of mixing processes. Particle image velocimetry (PIV) is a proven technique to derive velocity vector maps in a cross section of a fluid flow. Numerous examples are reported (Santiago et al. 1998; Meinhart et al. 1999; Devasenathipathy et al. 2003; Bourdon et al. 2004; Mouheb et al. 2011). An overview of recent advances is given by Wereley and Meinhart (2010). The velocity vectors are derived from sub-sections of the target area of the particle-seeded flow by measuring the movement of particles between two laser pulses. The exploited PIV mode here is called double frame/single exposure PIV and requires a camera which enables a fast frame transfer within the charge coupled device. PIV is a non-invasive whole-flow-field technique providing instantaneous velocity vector maps. To get a 3D insight of the interior region of the channel, there are some approaches to reach this, for example stereo imaging (Lindken et al. 2006; Wereley and Meinhart 2010) and multiple 2D image slices (Wereley and Meinhart 2010). The latter is applied in this work. A lot of experiments which refer to a mixing process use undistinguishable model fluids, e. g., shown by Lindken et al. (2006). The Raman and PIV measurements presented in the following are based on distinguishable fluids.

2 Experiments

2.1 Raman and PIV Setup

The entire setup using PIV and Raman spectroscopy is depicted in Fig. 1. The beam source and beam shaping optics are shared by the Raman and PIV part. First, the beam source and beam shaping optics are described.

The beam source consists of two identical Nd:YAG lasers (Continuum Surelite I-10, 4–6 ns pulsewidth) with doubling potassium phosphate crystals and 532 nm output wavelength. It also contains a beam-combining device which coordinates the beams coaxially. This technique causes, that the polarisation directions of the two linear polarised beams are orthogonal to each other. The resulting beam is divided by a beam splitter B1 into two ones. An arrangement like this is called double pulse laser system. The major part of its energy (probe beam) is transmitted through this beam splitter. This and all
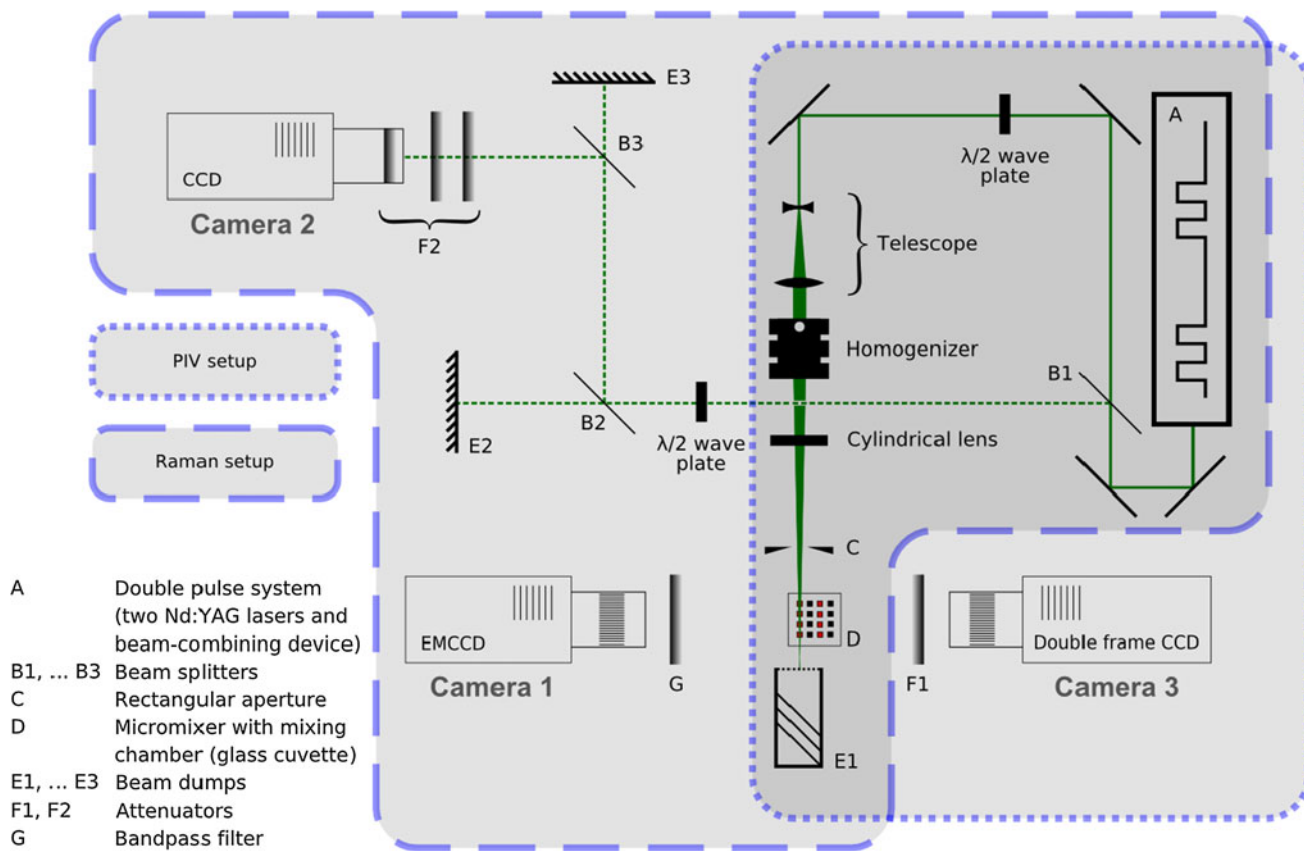
Fig. 1 Scheme of the combined Raman and particle imaging velocimetry setup. The probe beam is shown as *solid line* and the reference beam as *dashed line*

A	Double pulse system (two Nd:YAG lasers and beam-combining device)
B1, … B3	Beam splitters
C	Rectangular aperture
D	Micromixer with mixing chamber (glass cuvette)
E1, … E3	Beam dumps
F1, F2	Attenuators
G	Bandpass filter

other beam splitters are sheets of soda lime glass. Before the probe beam reaches the mixing chamber it is shaped by an imaging homogenizer. To generate a homogenous light sheet the beam is widened up to the diameter of the lens array LA1 (Fig. 2) by a telescope assembly. In this setup, micro lens arrays with cylindrical lenses (Linos, C-Q-500 2.5°) are applied. The first lens array LA1 in the beam path breaks up the beam into lots of small, divergent bundles of rays. In a short distance behind the focal plane of LA1 the lens array LA2 is localised. LA2 and the Fourier lens FL form the imaging optics which allocates homogenously the bundle of rays of LA1 over the height of the light sheet. The homogenising effect results from this allocation. Inhomogeneities caused, e. g., by hotspots in the incoming beam will be delocalized so that these will not appear in the light sheet. A high focal length ($f = 200$ mm) of the Fourier lens is chosen to minimize the variation of the sheet height along the beam axis. The divergence of the homogenizers output beam is still too great, so that the energy density at the mixing chamber is too low. This problem is eliminated by adding a cylindrical lens to the setup (Fig. 1). This cylindrical lens narrows the sheet to about 15 mm height in the area of the sample. This corresponds with the
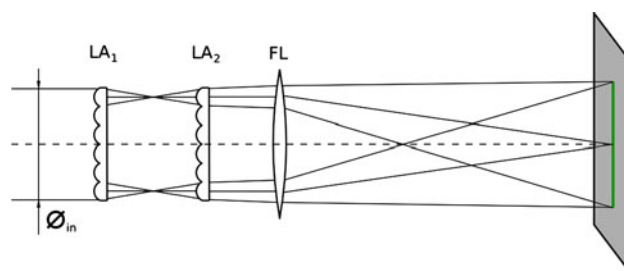

Fig. 2 Imaging homogenizer with the lens arrays (LA1 and LA2) and the Fourier lens (FL)

captured areas of camera 1 and camera 3. Finally, the width and height of the light sheet are ~ 300 μm and 15 mm, respectively. A scheme of the light sheet is depicted in Fig. 3 (right part).

The excitation or illumination of the sample is generated by two laser pulses which are added to increase the signal. The Raman-scattered light is detected by the highly sensitive EMCCD camera (Camera 1 in Fig. 1, Andor Technology, model iXon DU-897D). Using the bandpass filter G (LOT Oriel, 633FS10-25) the intensity and hence the concentration is monitored, as described in Sect. 3.
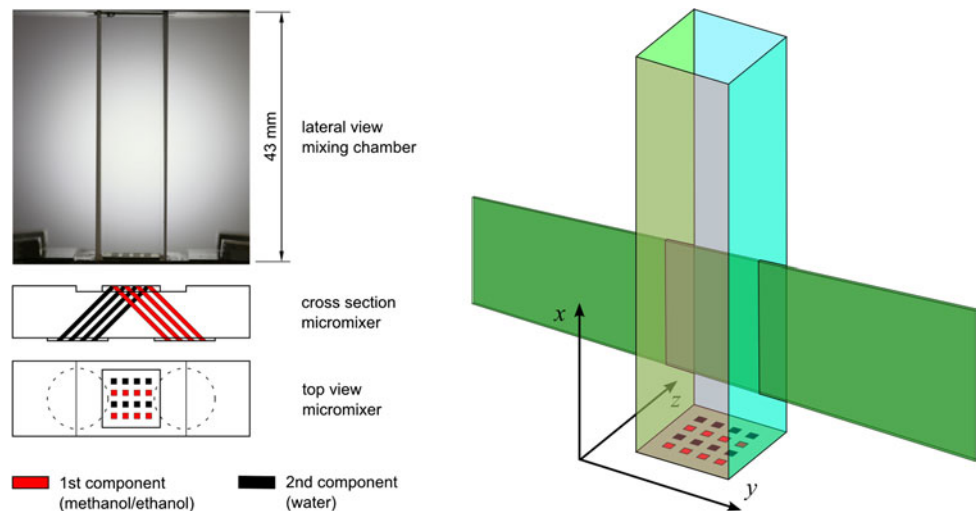
Unavoidable temporal fluctuations of the pulse energy of the Nd:YAG lasers cause deviations in the determination of the concentrations. This can be compensated by a comparison of the probe beam with a reference beam which is generated by beam splitter B1 and further attenuated by the beam splitters B2 and B3 and attenuators (F2) before it is projected on the lensless camera 2 (PCO, model Pixelfly qe).

To get velocity vector fields of the fluid flow, the measurements operate in the double frame/single exposure mode, a method which provides a single illuminated image for each illumination pulse. This method requires the double pulse laser system to generate a short-delay time Δt between two pulses and a frame transfer CCD with imaging optics called double frame camera. An advantage of double frame PIV is the preservation of the temporal order of the particle images and hence the directional unambiguousness. After the first laser pulse, the frame transfer CCD shifts the accumulated charge rapidly down into a masked-off area. The entire image can thereby be shielded from further exposure.

In case of the double frame mode, the following computing steps base on cross correlation. From the functional relationship between two successively recorded particle image frames, the local displacement can be derived. The velocity vectors are derived from sub-sections of the target area. These sub-sections, in PIV called interrogation areas, are rectangular areas of an edge length of a few pixels. Relating to the double frame mode, we get two successive intensity functions $I(i,j)$ and $I'(i,j)$ over an interrogation area. Taking account of discrete pixel maps, also the cross-correlation function can be termed discrete:

$$R(x,y) = \sum_{i=-K}^{K} \sum_{j=-L}^{L} I(i,j)I'(i+x,j+y). \quad (1)$$

Essentially the template I is linearly shifted around in the sample I'. For each choice of shift (x,y), the sum of the products of all overlapping pixel intensities produces one cross-correlation value $R(x,y)$. By applying this operation for a range of shifts, a correlation plane is formed. The better the particle images are aligned with each other, the higher the cross-correlation value R becomes. The algorithm searches over the whole correlation plane for the highest value R. The associated shift (x,y) indicates the local movement. This step is repeated for every interrogation area. The resulting map of vectors (x,y) is visualised as velocity vector map, when the frame interval Δt is known (Raffel et al. 1998).

The scattered light from the tracer ensemble is detected by camera 3, which is a double frame camera (La Vision 2D Messtechnik GmbH, model FlowMaster 3). The attenuator F1 protects camera 3 against pixel overflow and damage by intensive scattered light. A typical frame interval for relevant flow velocities of about 0.05 ms^{-1} is around 100 μs. The clock of the double pulse laser system is synchronized with the exposure of the two frames. The chronological order is managed by a programmable timing unit (PTU).

The beam-combining device causes orthogonal orientation of the polarisation planes. As the Mie scattering which is used for the detection is polarisation-dependent, the frame brightness of two successive frames would not be equal, which is not optimal for the advanced algorithm. This can be circumvented by introducing angle-adjustable wave plates. With this adjustment, the two beams are equal in their effect to illuminate the camera. Hence, the quality of the two frames is the same. The same applies to the reference beam. Unequal polarisation and the polarising effects of the beam splitters have also to be compensated by an angle-adjustable wave plate in the reference beam to obtain accurate Raman intensities.

Preliminary experiments have shown that the energy input caused by the laser light into the mixing liquids can lead to bubbling. The bubbles cause blooming and hence disturb recording of the images. Three measures are applied to prevent bubbling: Degassing of the liquids by vacuum in its pressure vessels, the use of membrane contactors (SuperPhobic®, Liqui-Cel) during the measuring mode and to pressurize the vessels with helium instead of air to drive the liquids through the hoses.

2.2 Micromixer

Figure 3 shows the principle construction of the micromixer and the mixing chamber. The micromixer consists of several plates which contain grooves at an angle of 45° and was made from an aluminium alloy (AlMg3, material code 3.3535). It has 8 channels in total for one passage and 8 channels in total for the other passage. In the cross section, the geometry of two times four channels is depicted. The top view shows the 16 outlets for the two components methanol/ethanol and water. This micromixer consists of 4 main plates (2 mm thick), each with 4-milled microchannels of 14.1 mm length, 0.9 mm width and 1.0 mm depth, which are separated 0.45 mm. Because of the angle of 45°, the outlet cross section of each microchannel is 1.27 mm wide and 1.0 mm high. In contrast to our usual micromixers with smaller microchannels (0.1 mm hydraulic diameter), where all foils are diffusion bonded, these plates are clamped so that the microchannels do not show deformations to avoid distortion of the flow profile. Furthermore, CFD calculations are faster with these larger microchannels than with smaller microchannels. The mixing chamber consists of a cuvette (inner cross section of 10 mm × 10 mm, height 43 mm) with open ends (Starna® 3Q10) made from fused silica, which is connected to the micromixer by a gasket. A sketch of the light sheet and the mixing chamber is shown in Fig. 3.

2.3 Chemicals

Water p. A. (AppliChem GmbH), ethanol for analysis (Merck KGaA) and methanol for analysis (Merck KGaA) were used. For non-fluorescent tracer particles, causing the Mie scattering, Polybead® Polystyrene Microspheres 1.0 micron and 10.0 micron from Polyscience, Inc. were used. Fluoresbrite® Carboxy NYO 1.0 micron and Fluoresbrite® Carboxylate Microspheres 6.0 micron Yellow Orange, made by Polysciences, Inc. were used as fluorescent tracer particles. During the experiments, we have not observed a decrease of the intensity of the fluorescent dyes.

3 Results and discussion

3.1 Mapping of species distributions

Raman spectroscopy enables the identification of molecules by their characteristic spectral parameters. Single-shot measurements exploiting the Raman effect have been used for characterization of fuel sprays before (Bazile and Stepowski 1994). Figure 4 shows the Raman spectra of water and ethanol. Whereas water shows broad bands at wavenumbers around 3,250 cm^{-1} caused by O–H stretching vibrations, characteristic C–H stretching bands of ethanol can be observed between 2,800 and 3,000 cm^{-1}. Additionally, in Fig. 4 the transmission curve of the interference filter is superimposed indicating the spectral area reaching the CCD camera. This signal is used to determine the spatial concentration of ethanol. Using this spectral area, a time resolution in the nanosecond time scale can be obtained due to the strong intensities of these Raman bands. The concentration field within the light sheet is frozen within a nanosecond time scale and all concentration values are measured simultaneously.

The scattering intensity I_j of a certain species of molecules j is described by the proportionality

$$I_j \propto I_0 \Omega V_D N_j \left(\frac{\partial \sigma}{\partial \Omega} \right)_j \lambda^{-4} \qquad (2)$$

with I_0 intensity of incoming exiting light, Ω solid angle of detection, V_D volume of detection, N_j number of molecules of the species j, $\left(\frac{\partial \sigma}{\partial \Omega} \right)_j$ Raman scattering cross section of the species j, λ excitation wavelength.

Considering a constant volume V_D it is possible to reduce Eq. (2) to the central and most important finding of the Raman part in the setup:

$$I_j \propto c^{(j)}, \qquad (3)$$

with $c^{(j)}$ as concentration of a species j. In a binary mixture, the detected total intensity $I(c^{(j)})$ only represents an affine function of the concentration $c^{(j)}$, because the other blend component causes an offset. The transmission curve of the interference filter prefers an area, where the signal of ethanol is maximal. To projecting the state of pure ethanol to the value 1, the offset of water will be eliminated by subtraction. To achieve this, the cuvette was filled with pure water. Camera 1 takes a series of images under real measuring conditions. The expression

$$\langle I^{\text{water}}(x,y) \rangle = \frac{1}{n} \sum_{i=1}^{n} I_i^{\text{water}}(x,y) \qquad (4)$$

leads to the average image $\langle I^{\text{water}}(x,y) \rangle$, represented by the position-dependent intensity $I^{\text{water}}(x,y)$, whereas n is the

Fig. 4 Raman intensity of ethanol and water (excitation wavelength 532 nm). Transmission spectrum of the interference filter G
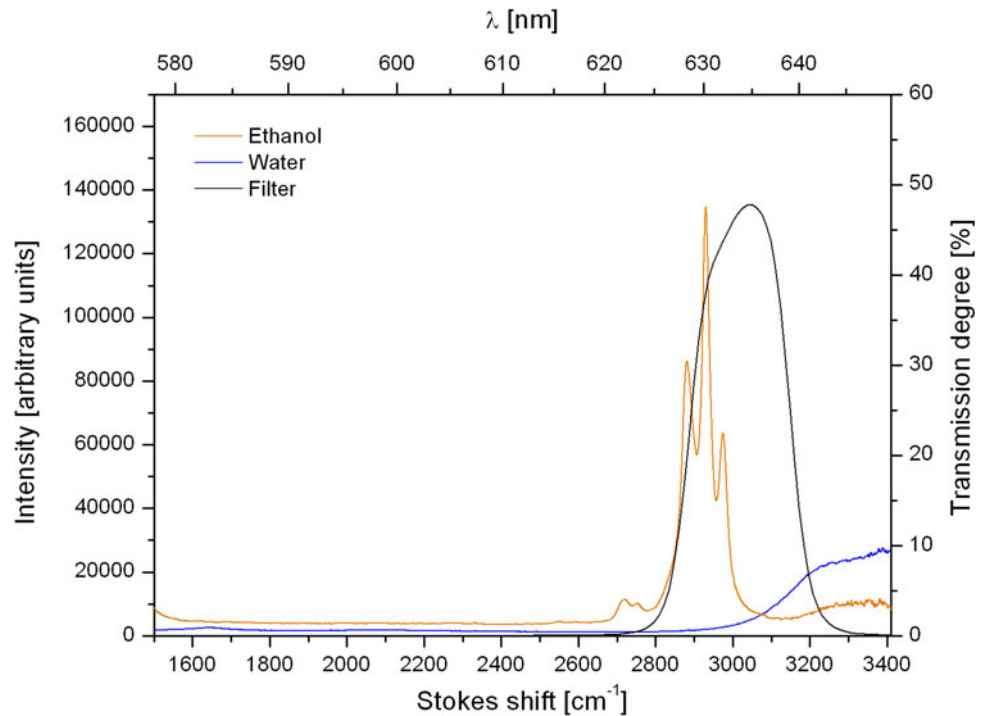
total of images. For the normalization, we have to calculate the difference of the intensities between water and ethanol.

$$\left\langle I^{\mathrm{diff}}(x,y)\right\rangle = \frac{1}{n}\sum_{i=1}^{n}\left(I_i^{\mathrm{EtOH}}(x,y) - I_i^{\mathrm{water}}(x,y)\right). \quad (5)$$

The normalization is achieved by division by Eq. (5). Considering Eqs. (3) and (4), the position-dependent concentration $c^{\mathrm{EtOH}}(x,y)$ of ethanol can be defined by

$$c^{\mathrm{EtOH}}(x,y) = \frac{I(x,y) - \frac{1}{n}\sum_{i=1}^{n}I_i^{\mathrm{water}}(x,y)}{\frac{1}{n}\sum_{i=1}^{n}\left(I_i^{\mathrm{EtOH}}(x,y) - I_i^{\mathrm{water}}(x,y)\right)}. \quad (6)$$

By this restriction, the values $c^{\mathrm{EtOH}}(x,y)$ are limited to the interval [0;1]. The concentration of water is determined by the complement $1 - c^{\mathrm{EtOH}}(x,y)$. The linearity of the measurement is experimentally verified in the study of Roetmann et al. (2008).

The light sheets of the mixing process of water and ethanol recorded by Raman imaging are shown in Fig. 5. They are taken successively and put together to depict the colour-coded distribution of concentration over the height of the cuvette. The colour range starts at black which implies 100% water and 0% ethanol and goes up to red implying the opposite. By rotating the probe around the vertical axis by 90°, a 3D view of the cuvette volume can be obtained. The small sketches indicate the light sheet position relative to the bottom of the micromixer with the fluid outlets. The volume flow-rate is $\dot{V} = 1.60$ l/h per component, conforming to

0.062 m/s flow velocity in a single channel. The Reynolds numbers, thus, are 58 and 39 for water and ethanol, respectively. Overall, the transitions from sheet to sheet are good as it can be observed at filaments and the spreading of the flow reflecting the quality of the analysis.

A detailed view shows that the ethanol filaments point according to the outlet angle of 45° to the left side. This can be observed in Fig. 5b, f where the light sheet is directly above the outlet. The laminar filaments curve close to the wall, where the ethanol concentration is low. Moreover, the filaments have obviously a tendency to trend to the centre (Fig. 5b–c, e–f, j–n). The filaments widen and go up to ca. 20 mm in height before a homogenous mixture is reached. The water injection points to the right side. A stream profile of the water cannot be recognized. However, the black and dark blue areas indicating water as the dominate species are mostly located on the right side conforming to the water outlets. Generally, on top the greenish area indicates a homogenous mixture of ethanol and water, whereas at the bottom besides at the ethanol outlets water prevails (Fig. 5k–r). The accumulation of water on the bottom agrees with computational fluid dynamics calculation taking into account the gravity and the difference in density of water and ethanol (Rinke et al. 2011a, b).

3.2 Velocity vector fields

One of the challenges in the field of mixing processes is to get information about the actual flow field and the
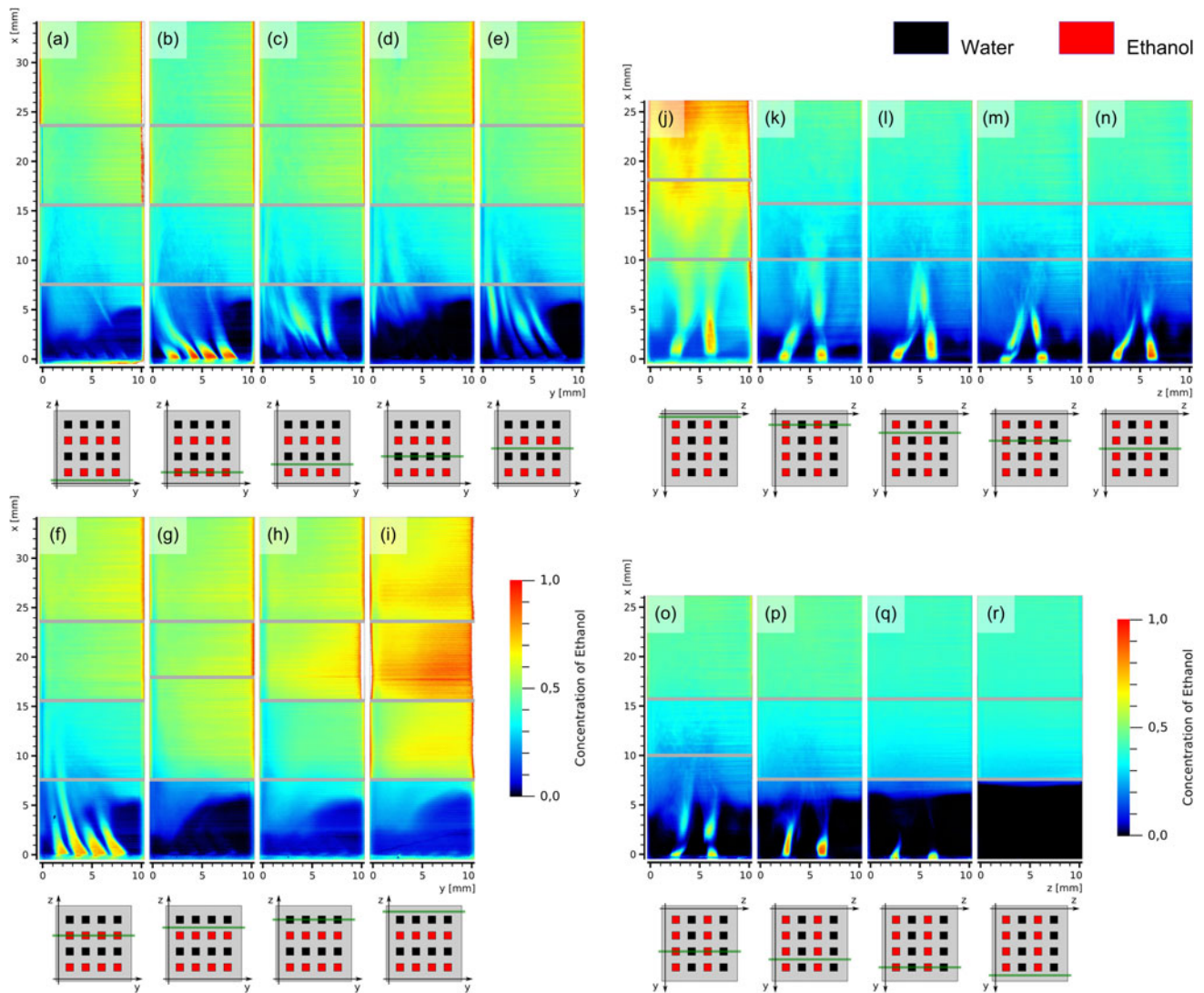
Fig. 5 Averaged Raman images of the concentration of ethanol and water in a mixing process, volume flow-rate: ethanol 1.6 l/h, water 1.6 l/h, laser sheet orthogonal to the *z* axis (*left*) and orthogonal to the *y* axis (*right*)

concentration of the species, simultaneously. Therefore a major issue of this study was to combine a PIV with a Raman setup to gain this information direct in the mixing chamber. For the PIV experiments microscopic tracer particles are added. The flow visualisation results from the visibility of these particles obtained by fluorescence or pure geometrical induced scattering. Respecting the applied particle size, the Mie theory provides the complete explanation in case of geometrical induced scattering (Raffel et al. 1998).

The fluids have to fulfil some requirements for PIV. First, the fluids have to be transparent because the detected intensities may not be dependent on the observation depth. Moreover, the liquids have to be available in a high-purity level, because foreign particles cause blooming, worsen the quality of the particle images and in rare cases bright

reflexes on particles can destroy areas on the CCD. Water, ethanol, and methanol in high-purity degrees fulfil these requirements.

The tracer particles which are added to the carrier medium must be taken with care. Oversized particles distort the flow and cause blooming. If the particles are too small, the excitation energy may not be sufficient to illuminate the double frame camera. The specific gravity of the particles has to be adapted to the liquids. Heavy particles underlie the slippage and can deviate from the local movement, while particles with low density refloat. The refractive index of tracers has to differ from the surrounding medium.

The selection of tracer material depends on the applied detection method such as geometrical scattering or fluorescence. In preliminary experiments appropriate tracers
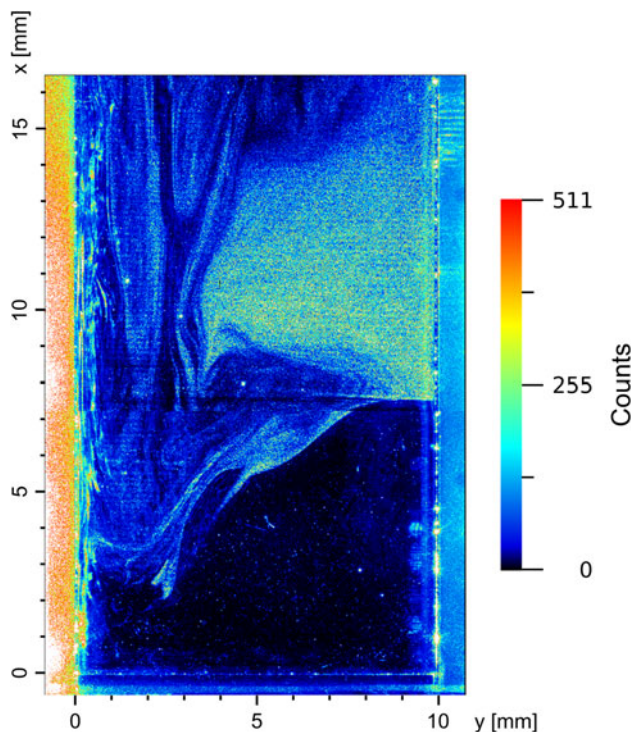
Fig. 6 Particle image of Polybead® Polystyrene Microspheres (1.0 μm) in the mixing process of methanol–ethanol mixture and water. The outlets of the micromixer are at the *bottom*

were found, e.g., the stability of the dyes and the solubility in the fluids were tested.

Figure 6 shows a particle image of Polybead® Polystyrene Microspheres. The scattered light from the particles is outshone by a parasitic light caused by schlieren. The latter are due to the heterogeneous gradient field of the refractive index of the two liquid components with $n_{D,1} \neq n_{D,2}$. As a

consequence, Mie scattering is inappropriate to record PIV images under these circumstances.

To solve this problem, we have adjusted the refractive index of ethanol by adding methanol to the refractive index of water (n_D = 1.33). Moreover, fluorescent tracer particles in combination with an optical filter with long-pass characteristics were used. The fluorescent light is transmitted by the optical filter, whereas the excitation wavelength is blocked. In short-test series, the best combination of filter and tracer material was evaluated. The combination for best applicability is Fluoresbrite® YO Carboxylate Microspheres, particle size 6.00 μm and a dichroitic long-pass edge filter, high reflective at 532 nm/45°. The importance of the particle size was emphasised by these tests. The resulting particle image is shown in Fig. 7 (left part). Its quality is well suited for PIV applications. The related mapping of the location-dependent fluid flow is depicted on the right sight. The PIV images were taken at the outlets of the methanol/ethanol mixture (laser sheet position z = 6 mm) and the resulting vector field conforms to the Raman image (Fig. 5f).

In short, the experimental setup is able to record the concentration distribution based on Raman imaging. The same setup can subsequently be used to obtain a PIV image, whereby a fluorescent tracer is added to the fluids. In the way, the comprehensive information of the concentration distribution and the flow profile can be combined for analysing the mixing process of fluids.

4 Conclusions and outlook

It has succeeded to develop a technique, which detects the species distribution and the velocity vector map during the
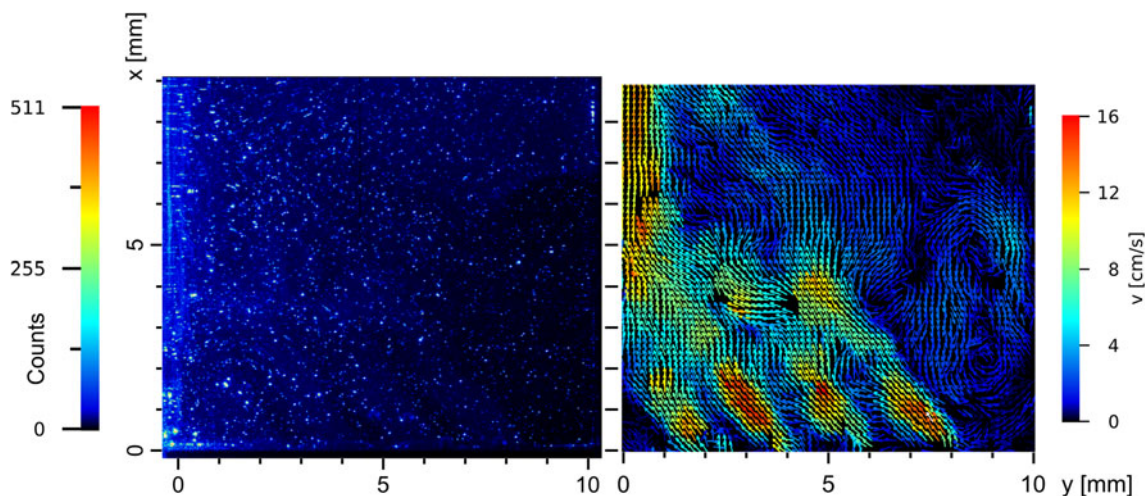

Fig. 7 Particle image of Fluoresbrite® Carboxylate Microspheres (6.0 μm) in the mixing process of methanol–ethanol mixture and water (*left*). The micromixer is placed at the *bottom*, volume flow-rate: methanol–ethanol mixture 1.8 l/h, water 1.8 l/h, velocity field (*right*)

mixing process. Using the example of an industry-oriented micromixer, it was shown, that the procedure copes complex structures of fluid flow with several filaments, too. Using high-sensitive EMCCD techniques, the system gets along with very-short integration times of about 5 ns. For a common multi-lamination mixer, the structure of the species distribution was observed from two perspectives in the mixing chamber above the outlets and the resulting colour-coded graphic is presented here. This method can be used for smaller devices, too. In this case, the laser sheet has to be made smaller using an appropriate lens system. Furthermore, the lens which images the Raman map onto the CCD camera has to be changed, too. The lateral resolution will be depend on the pixel numbers of the CCD camera.

The problem with outshining parasitic light in case of mixing distinguishable liquids was resolved by adequate choice of tracer material and a suitable optical filter in the PIV measurement.

This study shows the access to get information for a deeper understanding of the mixing process and will pave the way for the optimisation of CFD simulations. This enables the design and construction of effective micromixers.

References

Bazile R, Stepowski D (1994) Measurement of the vaporization dynamics in the development zone of a burning spray by planar laser induced fluorescence and Raman scattering. Exp Fluids 16:171–180. doi:10.1007/bf00206536

Beushausen V, Roetmann K, Schmunk W, Wellhausen M, Garbe C, Jähne B (2009) 2D-Measurement technique for simultaneous quantitative determination of mixing ratio and velocity field in microfluidic applications. In: Nitsche W, Dobriloff C (eds) Imaging measurement methods, NNFM 106. Springer, Berlin Heidelberg, pp 155–164

Bothe D, Stemich C, Warnecke HJ (2006) Fluid mixing in a T-shaped micro-mixer. Chem Eng Sci 61:2950–2958. doi:10.1016/j.ces.2005.10.060

Bourdon CJ, Olsen MG, Gorby AD (2004) Validation of an analytical solution for depth of correlation in microscopic particle image velocimetry. Meas Sci Technol 15:318–327. doi:10.1088/0957-0233/15/2/002

Deabate S, Fatnassi R, Sistat P, Huguet P (2008) In situ confocal-Raman measurement of water and methanol concentration profiles in Nafion® membrane under cross-transport conditions. J Power Sour 176:39–45. doi:10.1016/j.jpowsour.2007.10.044

Devasenathipathy S, Santiago JG, Wereley ST, Meinhart CD, Takehara K (2003) Particle imaging techniques for microfabricated fluidic systems. Exp Fluids 34:504–514. doi:10.1007/s00348-003-0588-y

Ewinger A, Rinke G, Kerschbaum S, Rinke M, Schubert K (2008) Raman-spectroscopy for measuring chemical reactions in mico reactors. In: Proceedings of the 6th international conference on nanochannels, micro channels, and minichannels, ICNMM (PART A), pp 747–748

Fair RB (2007) Digital microfluidics: is a true lab-on-a-chip possible? Microfluid Nanofluid 3:245–281. doi:10.1007/s10404-007-0161-8

Fletcher PD, Haswell SJ, Zhang X (2003) Monitoring of chemical reactions within microreactors using an inverted Raman microscopic spectrometer. Electrophoresis 24:3239–3245. doi:10.1002/elps.200305532

Hoffmann M, Schlüter M, Räbiger N (2006) Experimental investigation of liquid–liquid mixing in T-shaped micro-mixers using μ-LIF and μ-PIV. Chem Eng Sci 61:2968–2976. doi:10.1016/j.ces.2005.11.029

Hunt HC, Wilkinson JS (2008) Optofluidic integration for microanalysis. Microfluid Nanofluid 4:53–79. doi:10.1007/s10404-007-0223-y

Hüttner W, Christou K, Göhmann A, Beushausen V, Wackerbarth H (2011) Implementation of substrates for surface-enhanced Raman spectroscopy for continuous analysis in an optofluidic device. Microfluid Nanofluid. doi:10.1007/s10404-011-0893-3

Janasek D, Franzke J, Manz A (2006) Scaling and the design of miniaturized chemical-analysis systems. Nature 442:374–380. doi:10.1038/nature05059

Kölbl A, Kraut M, Schubert K (2008) The iodide iodate method to characterize microstructured mixing devices. AIChE J 54:639–645

Lee M, Lee JP, Rhee H, Choo J, Chai YG, Lee EK (2003) Applicability of laser-induced Raman microscopy for in situ monitoring of imine formation in a glass microfluidic chip. J Raman Spectrosc 34:737–742. doi:10.1002/jrs.1038

Leung SA, Winkle RF, Wootton RCR, deMello AJ (2005) A method for rapid reaction optimisation in continuous-flow microfluidic reactors using online Raman spectroscopic detection. Analyst 130:46–51. doi:10.1039/b412069h

Lindken R, Westerweel J, Wieneke B (2006) Stereoscopic micro particle image velocimetry. Exp Fluids 41:161–171. doi:10.1007/s00348-006-0154-5

Malarski A, Egermann J, Zehnder J, Leipertz A (2006) Simultaneous application of single-shot Ramanography and particle image velocimetry. Opt Lett 31:1005–1007. doi:10.1364/ol.31.001005

Meinhart CD, Wereley ST, Santiago JG (1999) PIV measurements of a micro channel flow. Exp Fluids 27:414–419. doi:10.1007/s003480050366

Mogensen KB, Klank H, Kutter JP (2004) Recent developments in detection for microfluidic systems. Electrophoresis 25:3498–3512. doi:10.1002/elps.200406108

Mouheb NA, Montillet A, Solliec C, Havlica J, Legentilhomme P, Comiti J, Tihon J (2011) Flow characterization in T-shaped and cross-shaped micro mixers. Microfluid Nanofluid 10:1185–1197. doi:10.1007/s10404-010-0746-5

Park T, Lee M, Choo J, Kim YS, Lee EK, Kim DJ, Lee SH (2004) Analysis of passive mixing behavior in a Poly(dimethylsiloxane) microfluidic channel using confocal fluorescence and Raman microscopy. Appl Spectrosc 58:1172–1179. doi:10.1366/0003702042336019

Raffel M, Willert C, Kompenhans J (1998) Particle image velocimetry—A Practical Guide. Springer-Verlag, Berlin

Rinke G, Ewinger A, Kerschbaum S, Rinke M (2011a) In situ Raman spectroscopy to monitor the hydrolysis of acetal in microreactors. Microfluid Nanofluid 10:145–153. doi:10.1007/s10404-010-0654-8

Rinke G, Wenka A, Roetmann K, Wackerbarth H (2011b) In situ Raman imaging combined with computational fluid dynamics for measuring concentration profiles during mixing processes. Chem Eng J. doi:10.1016/j.cej.2011.11.016 (in press)

Roetmann K, Schmunk W, Garbe CS, Beushausen V (2008) Micro-flow analysis by molecular tagging velocimetry and planar Raman-scattering. Exp Fluids 44:419–430. doi:10.1007/s00348-007-0420-1

Salmon JB, Ajdari A, Tabeling P, Servant L, Talaga D, Joanicot M (2005) In situ Raman imaging of interdiffusion in a micro channel. Appl Phys Lett 86:094106. doi:10.1063/1.1873050

Santiago JG, Wereley ST, Meinhart CD, Beebe DJ, Adrian RJ (1998) A particle image velocimetry system for microfluidics. Exp Fluids 25:316–319. doi:10.1007/s003480050235

Sauter EG (1996) Nonlinear optics. Wiley, New York

Sinton D (2004) Microscale flow visualization. Microfluid Nanofluid 1:2–21. doi:10.1007/s10404-004-0009-4

Viskari PJ, Landers JP (2006) Unconventional detection methods for microfluidic devices. Electrophoresis 27:1797–1810. doi:10.1002/elps.200500565

Walowski B, Hüttner W, Wackerbarth H (2011) Generation of a miniaturized free-flow electrophoresis chip based on a multi-lamination technique—isoelectric focusing of proteins and a single-stranded DNA fragment. Anal Bioanal Chem 401:2465–2471

Wereley ST, Meinhart CD (2010) Recent advances in micro-particle image velocimetry. Annu Rev Fluid Mech 42:557–576. doi:10.1146/annurev-fluid-121108-145427